HAL
open science

B→A allomorphic transition in native starch and amylose spherocrystals monitored by in situ synchrotron X-ray diffraction

Y. Nishiyama, J.L. Putaux, N. Montesanti, J.L. Hazemann, C. Rochas

To cite this version:

Y. Nishiyama, J.L. Putaux, N. Montesanti, J.L. Hazemann, C. Rochas. B→A allomorphic transition in native starch and amylose spherocrystals monitored by in situ synchrotron X-ray diffraction. Biomacromolecules, 2010, 11 (1), pp.76-87. 10.1021/bm900920t . hal-00447114

HAL Id: hal-00447114

https://hal.science/hal-00447114v1

Submitted on 1 Dec 2021

HAL is a multi-disciplinary open access archive for the deposit and dissemination of scientific research documents, whether they are published or not. The documents may come from teaching and research institutions in France or abroad, or from public or private research centers.

L'archive ouverte pluridisciplinaire **HAL**, est destinée au dépôt et à la diffusion de documents scientifiques de niveau recherche, publiés ou non, émanant des établissements d'enseignement et de recherche français ou étrangers, des laboratoires publics ou privés.

B→A allomorphic transition in native starch and amylose spherocrystals monitored by *in situ* synchrotron X-ray diffraction

Yoshiharu Nishiyama,[†] Jean-luc Putaux,[*,†] Nicole Montesanti,[†] Jean-Louis Hazemann,[‡] and Cyrille Rochas[¶]

Centre de Recherches sur les Macromolécules Végétales (CERMAV-CNRS), BP 53, F-38041 Grenoble Cedex 9, France - affiliated with Université Joseph Fourier and member of Institut de Chimie Moléculaire de Grenoble, Institut Néel, BP 166, F-38042 Grenoble Cedex 9, France, and Laboratoire de Spectrométrie Physique, UMR 5588, BP 87, F-38402 Saint Martin d'Hères, France

E-mail: jean-luc.putaux@cermav.cnrs.fr

Published in: **Biomacromolecules** 11 (2010), 76-87 - DOI: 10.1021/ma101794w

Abstract

The B→A phase transition in native starch granules and spherocrystals prepared from DP 20-40 synthetic amylose chains was investigated in situ at intermediate moisture content (20-30%) by wide-angle synchrotron X-ray scattering, using a temperature-controlled pressure cell. The transition in native starch was monitored at hydrostatic pressures of 1.6 to 11.0 MPa and occurred in a temperature range of 90-110°C. The transition temperature increased with increasing amylose content and the transition was incomplete in amylose-rich starch. The B→A

[†]CERMAV-CNRS, Grenoble
[‡]Institut Néel, Grenoble
[¶]Laboratoire de Spectrométrie Physique, Grenoble - current address: CERMAV-CNRS, Grenoble

transition in highly crystalline amylose spherocrystals was monitored at pressures between 2.0 and 28.5 MPa. The transition temperature was higher than in native starch, ranging from 125 to 135°C. At 2.0 MPa, after conversion, the hydrated spherocrystals melted at 185°C. Surprisingly, at the same pressure, in excess water, the spherocrystals did not solubilize but converted to allomorph A at 100°C and melted at 160°C. For all samples, the transition occurred in a matter of minutes and a higher pressure decreased the transition temperature. For the first time, thermal expansion coefficients were estimated for A- and B-amylose at intermediate moisture. A strong thermal anisotropy was observed for A-amylose, the expansion being higher along the *b*-axis than along the *a*-axis of the monoclinic unit cell. This anisotropy was attributed to the fact that, in the *b*-direction, amylose double helices lie at the same height along the chain axis while, in the *a*-direction, they are more closely packed in a zigzag fashion.

Introduction

Native starch occurs in the form of compact semi-crystalline granules and is mostly composed of a mixture of two homopolymers of glucose.[1] Amylopectin, the major component, is a branched macromolecule. The heterogeneous distribution of branching points results in a clustered organization of short linear branches, about 15 residues-long, that intertwine into double helices and form lamellar crystallites.[2,3] Amylose, the minor component, is mostly linear. It is generally amorphous in the granules but, to some extent, may also participate to crystallites.[4] Depending on the botanical source, the crystallites can adopt two different structures, namely A and B. Short-chain amylose can also be recrystallized *in vitro* from solutions upon cooling or addition of a precipitant, the resulting crystals yielding much more resolved diffraction diagrams. B-amylose crystallizes in pure water at low temperature whereas the crystallization of A-amylose occurs in the presence of acetone at 50-60°C.[1,5]

Molecular models of allomorphs A and B have been proposed based on X-ray diffraction data collected from fibers made of long-chain amylose.[6–10] The structure of allomorph A has been revised using electron diffraction data from single crystals prepared *in vitro* from short-chain amy-

lose[8,11] and, more recently, synchrotron X-ray microdiffraction data, also recorded from single crystals.[12,13] X-ray fiber diffraction data and conformational analysis[6–9] have suggested that a double-stranded helix was the building block of both A- and B-amylose crystals. The structures of both allomorphs differ in the conformation and packing of the double helices as well as in the number of water molecules included in the unit cell.[5]

In excess water, native starch granules swell and the crystallinity is irreversibly lost. The temperature at which this so-called 'gelatinization' occurs depends on the water content and is higher at smaller water contents. B-starch is known to convert into A-starch during a heat treatment at intermediate moisture (typically 20-35%).[14,15] No gelatinization occurs and the granular morphology is preserved.[16–18] This heat-moisture (HM) treatment is used in the industry to modify the physico-chemical properties of native starch (reduced swelling capacity or enhanced thermal stability in water, for instance). Variations on the HM treatment procedure have been recently proposed to improve the homogeneity of the transition in the batches of native starch processed at the industrial scale.[19,20]

The B→A transition was observed as well in the crystalline residues of acid-hydrolyzed potato and wrinkled pea starch containing chains with an average degree of polymerization (DP) of 15 and 30, respectively.[21] For potato hydrolysates, the onset temperature of the transition was in the same range as that measured for the parent granules but it was significantly higher with residues from wrinkled pea starch. The transition has also been carried out with products prepared by *in vitro* recrystallization of short-chain amylose.[22] The reverse transition from A- to B-type is considered to only occur when the sample has been completely gelatinized/dissolved and partially recrystallizes. However, Katopo et al. recently reported on a partial A→B transition in waxy maize starch submitted to a 690 MPa hydrostatic pressure.[23]

Despite a substantial number of studies, the mechanism of B→A conversion in starch is still unclear. Two hypotheses are still debated. On the one hand, allomorph B would dehydrate upon heating, resulting in a reorganization of the double helices into a more compact and less hydrated structure.[24] On the other hand, B-crystallites would melt and the chains would recrystallize into

allomorph A.[21]

In the recent years, synchrotron radiation has successfully been used to study structural transitions in starch. *In situ* series of small- and wide-angle X-ray scattering (SAXS and WAXS) spectra were recorded to monitor the variation in lamellar and crystal structure, respectively, during hydrothermal treatments. Several works focused on the structural transitions occurring in native starch granules in excess water[4,25–28] or limited moisture[29] conditions. Le Bail et al. also studied the formation of so-called V-type inclusion complexes with lipids in maize starch heated at intermediate and high moisture content.[30]

In the present paper, we report on temperature-resolved synchrotron X-ray diffraction experiments carried out at intermediate moisture in a pressure cell in order to investigate the kinetics of the B→A transition occurring in native starch granules and highly crystalline amylose spherocrystals.

Experimental

Sample Preparation. Potato amylopectin starch (PAPS, from Lyckeby Stärkelsen, Sweden)[31] and low- and high-amylose Dianella potato starch samples were gifts from E. Bertoft (Department of Biochemistry and Pharmacy, Turku University, Finland) and A. Blennow (Center for Molecular Plant Physiology, The Royal Veterinary and Agricultural University, Copenhagen, Denmark),[32] respectively. High-amylose Eurylon maize starch was provided by Roquette Frères (Lestrem, France). Banana starch was extracted from green plantain bananas purchased at a local market. The chemical and allomorphic compositions of all samples are summarized in supplementary Table S1.[33,34]

Amylose spherocrystals were prepared by crystallizing DP 20-40 synthetic amylose provided by S. Kitamura (Graduate School of Life and Environmental Sciences, Osaka Prefecture University, Japan).[35] A 2 wt% aqueous amylose solution was put into a glass vial, heated to 120°C in an oil bath for 45 min and filtered at 80°C through a 0.45 μm membrane filter to remove residual

aggregates. The clear solution was allowed to slowly cool down to 4°C. The resulting precipitate was air-dried and the powder kept for further use.

Scanning electron microscopy (SEM) images and polarized light micrographs of initial PAPS and Eurylon starch granules and amylose spherocrystals are shown in Figure 1 whereas images of initial Dianella and banana starch granules are presented in supplementary Figure S1. Powders of native starch granules and spherocrystals were poured into thin-walled borosilicate glass capillaries with a 1 mm outer diameter and allowed to equilibrate for a few days in a 95% relative humidity (r.h.) atmosphere at room temperature before being used for diffraction experiments.

Insert Figure 1

Optical and Scanning Electron Microscopy. Drops of starch granule and spherocrystal suspensions were deposited onto glass slides and observed between crossed polars at a magnification of 40× with a Zeiss Axiophot II microscope equipped with a λ compensator. Drops of the suspensions were also allowed to dry on copper stubs. The specimens were coated with Au/Pd and observed in secondary electron imaging mode using a JEOL JEM 6100 microscope operating at 8 kV.

Wide-Angle Synchrotron X-ray Scattering. As shown in Figure 2, a stainless steel specimen holder was designed to hold glass capillaries containing hydrated or wet starch granules or spherocrystals (Figure 2a). The upper end of the capillaries was open during the experiments. Water was placed in a surrounding container, not in direct contact with starch, to prevent dehydration of the sample in the pressurized He environment. The specimen holder was inserted in a sapphire tube (Figure 2b) and placed inside the cell equipped with two 0.8 mm-thick sapphire windows (Figure 2c). A detailed description of the pressure cell can be found in the paper by Testemale et al.[36] The chamber was filled with He gas and the pressure was regulated in a range of 2 to 30 MPa (±0.1 MPa).[37] The samples and water containers were then heated at temperatures between 25 and 180°C (±0.1°C) using a Eurotherm controller.

Insert Figure 2

The samples were probed by a 24 keV (λ = 0.05179 nm) X-ray beam on the BM02 beamline of the French CRG at the European Synchrotron Radiation Facility (ESRF, Grenoble, France). WAXS patterns were recorded using a CCD detector during 30 to 200 s exposures, with an angular range of ±11° defined by the diameter of the exit window of the pressure cell (Figure 2d).

The optical distortion of the camera was corrected using a program developed at the beamline. The divergence of the beam was significantly smaller in the vertical direction compared to horizontal direction, judging from the peak width in the diffraction patterns of the highly crystalline amylose spherocrystals. Consequently, radial profiles were calculated by integrating a fan-shaped area in the vertical direction of the ring pattern.

The diffuse background due to scattering from air, pressurized He and pressure cell windows was approximated by a linear combination of two exponential functions and one linear function:

$$f(x) = a_0 \exp(-a_1 x) + a_2 \exp(-a_3 x) + a_4 x + a_5 \tag{1}$$

This function was fitted against the data using a maximum entropy approach, as described by von der Linden et al.[38]

Results

B→A Transition in Native Starch Granules

The initial WAXS spectra of PAPS, low- and high-amylose Dianella and Eurylon starches were typical of B-starch, with two characteristic strong peaks located at q = 0.4 and 1.2 Å^{-1} (d-spacing = 16 Å and 5.2 Å, respectively). 16 Å is the distance between the 100 crystallographic planes in the hexagonal unit cell of B-amylose, and thus the peak at q = 0.4 Å^{-1} will be referred to as 100_B in the following. Banana starch exhibited a C-type spectrum, typical of a mixture of allomorphs A and B (supplementary Table S1).

All samples of hydrated native starch granules were heated up to 120 or 140°C at a rate of

about 3°C/min, under pressures ranging from 8.5 to 11.0 MPa. Figure 3 compares the evolution of the WAXS profile of each sample with temperature. The diffraction peaks never disappeared completely within the explored temperature range. However, the intensities of the peaks characteristic of B-starch drastically decreased above 70°C. The position and intensity of the 100_B peak were fitted at each temperature using pseudo-Voigt functions and a nonlinear least-squares method. The intensity values are plotted in Figure 4.

Insert Figure 3

Upon heating at 8.5 MPa, the B-type profile of hydrated PAPS granules was clearly recognized up to 100°C (Figure 3a). There was a slight shift of the 100_B peak to lower q-values with increasing temperature due to thermal expansion. The intensity of 100_B significantly decreased between 100 and 110°C and reached zero (Figure 4a). The sample was heated up to 120°C and cooled down to room temperature. No transition was observed upon cooling but the intensity of the peaks significantly increased and the final profile was clearly that of A-starch. A comparison of the initial B-type and final A-type powder diffraction patterns at room temperature is shown in supplementary Figure S2a.

When PAPS granules were heated at 1.6 MPa, the general behavior was similar to that observed at 8.5 MPa (Figure 3b) but there was a slight increase of the temperature at which the intensity of 100_B started to drastically decrease (75°C) and finally reached zero (115°C) (Figure 4b).

Insert Figure 4

The SEM images of PAPS granules after the HM treatments did not reveal any significant change in morphology (Figures 5a and 5c). The birefringence pattern in polarized light micrographs was generally similar to that of native granules. The molecular orientation appeared to be preserved and no swelling associated to gelatinization was detected. However, some limited damage was observed, located at the hilum of some granules, in the form of small regions where the birefringence was lost (Figures 5b and 5d).

Insert Figure 5

Upon heating at 8.8 MPa, low-amylose Dianella starch behaved like PAPS (Figures 3c and 4c, supplementary Figure S2b) whereas the transition was much less clearly identified in high-amylose Dianella and Eurylon starch (Figures 3d and 3e, respectively). In particular, for Eurylon starch, the intensity of the 100_B peak significantly decreased between 120 and 140°C but never reached zero (Figure 4e). In high-amylose Dianella starch, a A-type profile could only be identified after cooling down to room temperature when the peaks regained a sufficient intensity (Figure 3c and supplementary Figure S2c). In Eurylon starch, the A-type profile could not be clearly recognized even after cooling. A peak at $q = 0.55$ Å^{-1} was present in all spectra (even for the inital sample) and did not evolve with temperature. Its origin is unknown and the reflection may be due to some contaminant. However, two sharp peaks at $q = 0.95$ and 1.4 Å^{-1} appeared at 140°C and remained upon cooling. They are likely due to the formation of a small amount of V_H complexes between amylose and lipids. A similar effect has been observed during the heating of maize[30] and rice[29] starch at about 150°C in limited moisture.

SEM and polarized light micrographs of low- and high-amylose Daniella starch after the HM treatments are shown in supplementary Figure S3. In both cases, the shape and molecular orientation of the granules were preserved and small cavities could be seen at the hilum of Dianella granules, the larger damage being observed for the low-amylose sample (Figure S3d). In the case of Eurylon, we did not see any cavity in the granules (Figures 5e and 5f).

Upon heating, the diffraction profiles of hydrated banana starch granules changed from initial C-type to pure A-type (Figure 3f and supplementary Figure S2e). The transition of the B-crystallites occurred between 80 and 120°C (Figure 4f). The morphology and optical birefringence pattern were preserved after the treatment and only very small cavities were observed at the hilum of the granules (Figures S3e and S3f).

B→A Transition in Synthetic Amylose Spherocrystals

Initial Allomorphic Composition of the Spherocrystals

Profile I in Figure 6 corresponds to the WAXS spectrum of the initial spherocrystals recorded at room temperature. Several peaks, indicated by arrows, could not be assigned to a B-type hexagonal unit cell. These peaks suggested that a certain amount of A-type crystallites was present in the sample. This was confirmed after performing a HM treatment that converted the sample to pure A-amylose (Figure 6, profile IV).

Insert Figure 6

The intensity profiles of A-amylose calculated from atomic coordinates published by Imberty et al.[8] and, more recently, by Popov et al.,[13] are shown as profiles V and VI in Figure 6, respectively. The peak positions in profile V were close to those in our experimental profile I but the relative intensities were rather different. The structure proposed by Popov et al. gave a satisfactory fit for intensity distribution but the peak positions were significantly different, probably due to the fact that the data of Popov et al. were collected at 100 K, resulting in a contraction of the unit cell and thus a shift of the diffraction peaks to larger q-values. Due to the limited spatial resolution and overlapping of reflections, the indexation of peaks was not obvious. Therefore, we used a simulated annealing method to refine the unit cell parameters against our experimental profile IV (Figure 6).

Assuming that the initial sample indeed contained a fraction of A-amylose, the A-type profile obtained from the same sample after total conversion (profile IV) was subtracted from profile I after multiplication by a scaling coefficient. The peaks assigned to allomorph A in profile I disappeared when the A-type spectrum was subtracted with a scaling coefficient of 0.3, which meant that the initial spherocrystals contained about 30% of A-type crystallites.

After the weighted subtraction of the A-type profile, the B-type spectrum of the initial sample could be completely fitted using a hexagonal unit cell (profile II in Figure 6). Since only

two parameters are required to define a hexagonal unit cell, the positions of two individual and independent peaks, namely 100_B and 111_B, were used to determine the unit cell parameters.

The intensity profile of B-amylose generated from the model of Imberty and Pérez[9] is shown in Figure 6 (profile III). There is a shift of most peaks towards smaller q-values which means that the reported unit cell, previously determined by Wu and Sarko from diffraction data collected from amylose fibers,[6] was larger than ours. However, the overall intensity distribution in the simulated profile was similar to our experimental data, indicating that the structure at our experimental resolution (about 0.3 nm) would be quite close to that of Imberty and Pérez.

Insert Figures 7, 8 and 9

B→A Transition

Transition in Hydrated Conditions. A first experiment was carried out by heating hydrated spherocrystals at a rate of 5°C/min from 20 to 160°C, at a pressure of 8.5 MPa. As seen in the series of WAXS profiles shown in Figure 7a, upon heating, the presence of allomorph B is clearly recognized up to 140°C. There is a slight shift of the peaks to lower q-values with increasing temperature due to thermal expansion. Contrary to what was observed on PAPS granules heated at the same pressure, the intensity of the peaks did not significantly decrease at high temperature until the transition occurred. The intensity of the characteristic 100_B peak started decreasing at about 115°C and reached zero at 145°C (Figure 8a). At 160°C, the sample was cooled down to room temperature and the intensity of the diffraction peaks increased. The spectrum of allomorph A contained about 20 peaks up to a 0.3 nm resolution (supplementary Figure S4a). A second heating/cooling cycle was performed up to 160°C in order to study the thermal behavior of pure allomorph A in this temperature range.

A similar HM treatment was performed at 28.5 MPa, up to 160°C (Figure 7b). The intensity of 100_B started decreasing at about 110°C and reached zero at 140°C (Figure 8a). The intensity of the resulting A-type profile significantly increased after cooling to room temperature (not shown).

SEM images and polarized light micrographs of the sample HM-treated at 8.5 MPa are shown

in Figures 9a and 9b. Those recorded from the sample treated at 28.5 MPa were very similar (not shown). The initial sample was constituted of aggregated 1-5 μm spherical particles (Figure 1e). Due to this aggregation, the birefringence pattern was complex and could be described as a juxtaposition of regions with specific polarization colors (Figure 1f). The aggregation of the HM-treated particles was more pronounced, with signs of partial fusion at the surface of the particles (Figure 9a). However, the optical birefringence patterns remained similar (Figure 9b).

A third experiment was carried out on hydrated spherocrystals at 2.0 MPa. The sample was first heated up to 105°C (5°C/min), a temperature below that of the B→A transition, then cooled down to room temperature. This treatment was repeated once. These two cycles allowed recording data on the thermal properties of allomorph B upon heating and cooling. The diffraction profile collected after the second heating cycle was similar to those recorded after the first heating cycle and from the initial sample, which meant that the heat treatments carried out at limited moisture did not produce any annealing effect. Then, the sample was heated up to 160°C. The corresponding series of diffraction profiles is presented in Figure 7c. The intensity of the 100_B peak started decreasing at 115°C and reached zero at about 155°C (Figure 8b). The intensity in the profile of the resulting A-amylose significantly increased upon cooling to room temperature. A new heat treatment was then performed up to 185°C and the diffraction pattern disappeared due to the melting of A-amylose crystals.

Transition in Wet Conditions. An experiment was set up to perform B→A then A→B transitions on the same sample. The A→B transition was expected to only occur after a melting/dissolution of the sample in excess water and its partial recrystallization upon cooling. Our treatment was thus performed with spherocrystals initially soaked in water, at 2.0 MPa. Upon heating, the intensity of the 100_B peak started decreasing at about 75°C and reached zero at about 125°C (Figures 7d and 8b). Simultaneously, the intensity of the peak from A-amylose located at $q = 1.62$ Å^{-1} increased, reaching a maximum at 125°C. Then, the intensity decreased again upon heating to 160°C when the diffraction pattern totally disappeared due to the melting/dissolution of the crystallites. After a

20 min rest at room temperature, a strong diffraction pattern reappeared, containing 28 peaks from allomorphs A and B up to a resolution of 0.3 nm (supplementary Figure S4b).

The SEM images and polarized light micrographs of the specimen retrieved after the experiment are shown in Figures 9c and 9d. While the aggregated particles are still spheroidal, with a 3-4 μm average diameter, their surface aspect is clearly textured (Figure 9c) and each particle exhibits uniform polarization colors (Figure 9d). This result is similar to what was observed on axialitic particles prepared by crystallization of amylose enzymatically-synthesized *in vitro* at 30°C by amylosucrase from 600 mM sucrose.[39] The authors reported that the average DP of the amylose chains in the particles was 35 which corresponds well to the range of DP of the fraction of synthetic amylose (20-40) used to prepare our spherocrystals.

Discussion

The fact that the B→A transition was successfully achieved with samples of native starch granules and amylose spherocrystals validates our experimental set-up. A sufficient hydration was preserved during the heat-pressure treatments, thanks to the water container. Although our set-up did not allow monitoring the hydration level in the cell during the treatments, the 20-30% moisture initially achieved by equilibrating the samples in a 95% r.h. atmosphere and necessary for the transition to occur do not seem to have significantly changed.

For both native starch granules and amylose spherocrystals, the transition was rather fast, occurring in a matter of minutes, as was reported for potato starch hydrolysates,[22] in contrast with the HM treatments of various starches reviewed by Jacobs and Delcour[17] and that generally last several hours. This can be explained by the fact that we used 1 mm-wide capillaries whereas during bulk transformation, wider glass tubes have been used. Hydrated starch has a high thermal capacity, c = 2.5 $\mathrm{Jg^{-1}K^{-1}}$,[40] and a low thermal conductivity, k = 0.38 $\mathrm{Wm^{-1}K^{-1}}$.[41] The bulk density of the powder can be estimated to 0.7×10^{6} $\mathrm{gm^{-3}}$.[42] The heat diffusivity $\kappa = \frac{k}{c\rho}$ is thus about $2.2\times10^{-7}\mathrm{m^2s^{-1}}$. A rough estimation of the time necessary to equilibrate within 10% of the

temperature increment over the whole capillary is of the order of minutes, whereas the content of a glass tube of 1 cm diameter would rather take hours to equilibrate. Our thin capillaries allowed a reasonably fast and homogeneous thermal equilibration considering the heating rate that was applied (3-5°C/min). For bulkier samples submitted to a static heating, a high temperature gradient would cause water migration, resulting in a heterogeneous structural transition.

B→A Transition in Native Starch Granules

The transition temperature was determined by monitoring the variation of the 100_B peak intensity and defined as $T_{trans} = 1/2(T_{final}\text{-}T_{start})$. The values of T_{start}, T_{trans} and T_{final} determined for all experiments are summarized in supplementary Table S2. The transition temperatures for PAPS treated at 1.6 and 8.5 MPa are 95±5 and 90±5°C, respectively. Thus, when amylose is not involved, the transition temperature would increase with decreasing pressure. However, considering the limited precision and number of experiments, the differences may not be significant. For samples containing amylose, regardless of the pressure (varying from 8.8 to 11.0 MPa), the transition temperature tends to increase with increasing amylose content: 100±5°C for low-amylose Dianella starch (2 wt% amylose), 100±5°C for banana starch (28 wt% amylose), 110±5°C for high-amylose Dianella starch (40 wt% amylose). Although the intensity of peak 100_B had decreased by half at around 120°C, no transition temperature could be unambiguously determined for Eurylon starch (70 wt% amylose) as no clear build-up of a A-type signal was observed. A high amylose fraction would thus apparently hinder the B→A transition. If, as suggested by Jenkins et al.,[4] amylose disrupts the structural order in amylopectin crystallites to some extent, long amylose chains may lack the mobility that is necessary to facilitate the reorganization of double helices during the structural transition at limited moisture.

The range of pressure explored in our experiments (1.6-28.5 MPa) was much lower than that used by various authors to study pressure-induced gelatinization of native starch granules in excess water and which typically extended up to 500-750 MPa.[43–46] Liu et al. have recently shown that waxy maize starch granules submitted to a 10 MPa pressure did not exhibit any discernable

morphological or structural change.[47] Consequently, during our experiments, we did not expect to observe any damage corresponding to a partial pressure-induced gelatinization. However, in all samples, with the exception of Eurylon, small cavities were observed at the hilum of HM-treated granules, although they were not present in all granules of a given specimen. A similar "damage" was reported by Kawabata et al.[48] and Vermeylen et al.[28] in HM-treated potato starch granules. The fact that these regions presented no birefringence in polarized light micrographs was not sufficient to conclude on their nature. The SEM images of broken granules by Kawabata et al. unambiguously showed that they were cavities and not disordered material.[48] We reached the same conclusion by observing air bubbles entrapped in the cavities immediately after HM-treated granules had been soaked in water (supplementary Figure S5). The origin of the cavities is still unclear. Kawabata et al. suggested that a mechanism similar to leaching in limited moisture occurred, corresponding to a partial migration of amylose to the outer layers of the granules. However, we have observed similar cavities in amylopectin-rich granules and they were the largest for low-amylose Dianella starch. As we did not detect any clear correlation of cavity size with pressure, the damage may rather be related to a lower crystallinity and/or a higher hydration level in the hilum region.[45]

B→A Transition in Amylose Spherocrystals

The reason why the initial spherocrystals contained a fraction of A-type crystallites is not clear. The initial synthetic amylose powder may have not completely dissolved because the temperature was not high enough or stirring was insufficient. Aggregates smaller that the filter porosity may have then acted as nuclei for crystallization. Some A-type crystallites would have formed at high temperature, B-amylose then crystallizing at lower temperature. Nevertheless, the sharpness of the diffraction profiles and the possibility to separate the signals associated with A- and B-amylose allowed performing a thorough analysis of the data.

As previously described for native starch samples, the B→A transition temperature of amylose spherocrystals was evaluated by considering the midpoint of the 100_B reflection intensity decrease. The characteristic temperatures determined for the four experiments are listed in supplementary

Table S2. In hydrated conditions, the temperature range during which the intensity of 100_B decreased was similar to that observed for native starch granules, *i.e.*, about 30-40°C (Figures 4 and 8). This value is in good agreement with that determined from the endotherm in the differential scanning calorimetry (DSC) thermogram of lintnerized potato starch at 35% moisture.[21] However, it decreases with increasing pressure (40°C at 2.0 MPa and 30°C at 28.5 MPa). The transition temperature also decreases with increasing pressure, from 135±5°C at 2.0 MPa to 125±5°C at 28.5 MPa. These results suggest that a higher pressure promotes the structural transition.

The transition temperature of hydrated amylose spherocrystals (125-135±5°C) was significantly higher than that of native starch samples (90-110±5°C) and higher than that measured in crystalline residues from acid-hydrolyzed potato starch (DP 15):[22] from 90 to 130°C for 40 to 20% moistures, respectively. However, the chain length and crystallinity of lintnerized potato starch limit dextrins were smaller than in our case. In addition, it has been shown that within the same hydration range (40-20%), the transition temperature range shifted to 145-160°C, respectively, for residues from acid hydrolyzed pea starch with DP 30.[21] This is in agreement with our data collected from DP 20-40 amylose spherocrystals and indicates that a higher chain length increases the transition temperature.

When the spherocrystals were heated in excess water, we did not observe any dissolution of the B crystallites. Instead, the B→A transition first occurred and then A-amylose dissolved at 160°C. This was highly surprising since such a phenomenon had never been reported in previous works. However, the transition temperature dropped to 100±5°C, which may illustrate a plasticizing effect of excess water. A similar behavior was reported for the I_α(triclinic)→I_β(monoclinic) phase transition in native cellulose: the transition occurred at 260˚C in excess water and 280˚C in an inert atmosphere.[49]

In addition, at 2.0 MPa, after transition, the A-amylose spherocrystals melted at 185°C and 160°C in hydrated and wet conditions, respectively. These values are significantly higher than that reported by Whittam et al. (74°C) for A-type spherocrystals prepared from DP 15 potato starch limit dextrins heated in excess water.[50] Ring et al. studied the behavior of B-type spherulites

prepared from DP 22 amylose in water. Using DSC, the authors detected an endothermal peak at 74°C but did not mention any phase transition.[51] Moates et al. have studied the effect of chain length on the melting temperature of B-amylose at a water volume fraction of 0.8.[52] The position of the endotherm suggested that the melting temperature increased from 57 to 119°C when the DP of amylose increased from 12 to 55, respectively, but the authors did not mention any other transition preceeding melting. More recently, Crochet et al.[53] showed that A-type spherulites prepared from DP 15 potato limit dextrins melted at a temperature of 90-100°C, for a starch-to-moisture ratio of 0.2-0.5. The increase of the melting temperature with increasing chain length has already been demonstrated at intermediate moisture for crystalline products prepared from limit dextrins[21] and synthetic amylose.[52] However, so far, the effect of pressure on starch has only been studied in the case of gelatinization at high pressure whereas the influence of pressure on structural transitions and melting has not been documented.

Thermal Expansion Coefficients of A- and B-amylose

In order to evaluate the thermal expansion coefficients of allomorphs A and B, we calculated the unit cell parameters from each diffraction profile and plotted their evolution with temperature. Only data from amylose spherocrystals were used since the diffraction peaks could be located with a high precision. The parameters of B-amylose were calculated using the position of independent 100_B and 111_B peaks, whereas those of A-amylose resulted from a fit of the whole diffraction profile.

A symmetrical thermal strain tensor was derived from the variation of the unit cell parameters after a change of temperature.[54] The expression of each component of the tensor is detailed in supplementary Equations S1 and S2. The principal components of the strain tensor, *i.e.*, the linear thermal expansion coefficients ε_1, ε_2 and ε_3 were calculated using supplementary Equations S3. The ε_1-axis is defined as normal to the *c*-axis and makes an angle ϑ clockwise with the *b*-axis (supplementary Equation S4). The ε_2-axis is normal to both the ε_1- and *c*-axis and the ε_3-axis is parallel to the *c*-axis. For a given set of (ε_1, ε_2, ε_3, θ), a corresponding ellipsoid is defined to

characterize the anisotropy of the thermal expansion.

The evolution of the unit cell parameters of B-amylose before the B→A transition and A-amylose after the transition is shown in Figure 10. The plots compile the values calculated from the four experiments described in the Results section, upon heating or cooling both allomorphs. In general, the data superimpose rather well.

Insert Figure 10

Between room temperature and 120°C, the unit cell of hydrated A- and B-amylose expanded linearly along the *a*- and *b*-axis but contracted along the *c*-axis, parallel to the double helices. The *a*-parameter increased by 0.10/0.15 Å, corresponding to an expansion of 0.6/0.8%. In the same temperature range, the *c*-parameter decreased by 0.05/0.15 Å, corresponding to a contraction of 0.5/1.5%. The linear thermal expansion coefficients along the *a*- and *c*-axis were thus 60-80 ppm and -50/-150 ppm/K, respectively (supplementary Table S3). The increase of the monoclinic angle γ and decrease of the fiber period *c* was larger at higher pressure (28.5 MPa). The reason of the contraction along the *c*-axis is not known with precision. In the absence of a detailed molecular dynamics study of the phenomenon, we can only assume that the heating of the hydrated crystals provides more conformational freedom around the glycosidic bonds and also infleunces the hydrogen bonding scheme. A similar effect was reported by Hori et al. during the heating of populus wood.[55] The unit cell of cellulose was shown to expand along the *a*- and *c*-axis while it contracted along the *b*-axis.

Using supplementary Equations S5 and S6, the thermal expansion coefficient $\varepsilon_{a,b}$ in the (*a*,*b*) plane was calculated for A- and B-amylose. Within the considered temperature range, a value of $\varepsilon_{a,b}$ = 130 ppm/K was found for both allomorphs.

Insert Figure 11

At 2.0 and 8.5 MPa, the long axis of the ellipse determined for the newly formed hydrated A-amylose was almost parallel to the *b*-axis, with an amplitude of ε_2 = 110 ppm/K, whereas the thermal expansion coefficient orthogonal to this direction was ε_1 = 12 ppm/K (Figure 11d). The

anisotropy was constant over the whole investigated range of temperature. At 28.5 MPa, two different behaviors were observed. Below 120°C, the anisotropy was lower, with ε_1 = 40 ppm/K and ε_2 = 105 ppm/K. Above 120°C, the anisotropy was higher, with ε_1 = 16 ppm/K and ε_2 = 170 ppm/K (Figure 11d). In both cases, though, the long axis of the thermal expansion ellipse was perfectly parallel to the *b*-axis. The linear thermal contraction along the *c*-direction was also higher at 28.5 MPa (supplementary Table S3). A higher pressure thus seems to favor a smaller monoclinic angle and *c*-parameter.

In wet conditions, at 2.0 MPa, the thermal behavior of B-amylose below the transition temperature was similar to what was observed at 28.5 MPa in hydrated conditions, suggesting that a higher pressure or an excess of water have a similar effect. However, above 120°C, after the transition, the unit cell of A-amylose exhibited a very different behavior from that observed in hydrated conditions. The *a*-axis contracted while the *c*-axis expanded, which is the opposite to what occurred to hydrated B- and A-amylose. From the transition at 120°C to the melting at 150°C, the unit cell volume increased by 30 $Å^3$ (supplementary Figure S6) which approximately corresponds to the volume of one water molecule. The excess water that solubilizes the ends of the chains might have the effect of physically pulling the amylose chains, resulting in a slight extension.

The thermal expansion coefficients determined for A- and B-amylose are of the same order of magnitude as those measured from other polysaccharide crystals. A clear anisotropy was observed for cellulose I_β (43-170 ppm/K along the *a*-axis and 5 ppm/K along the *b*-axis in the monoclinic unit cell) and cellulose III_I (76 ppm/K along the *a*-axis and 8 ppm/K along the *b*-axis in the monoclinic unit cell).[56] α-chitin exhibited a quasi-isotropic expansion of about 60 ppm/K along the *a*- and *b*-axis in the orthorhombic unit cell, whereas the thermal expansion of anhydrous β-chitin was anisotropic (40 ppm/K along the *a*-axis and 30-146 ppm/K along the *b*-axis in the monoclinic unit cell).

Molecular Description of the B→A Transition

In the current crystallographic models of A- and B-amylose, the main difference between the two allomorphs lies in the packing of the double helices and the number of included water molecules. In B-amylose, the 3 neighboring double helices are separated by 10.4 nm and translated by *c*/2 along the *c*-axis (Figure 11a).[9] The interaction between double helices is obviously favored in this staggered organization due to a better nesting. In A-amylose, the zigzag arrangement of double helices is only preserved in the *(a,c)* plane, with an inter-helix distance of 10.4 nm. In the *(b,c)* plane, the duplexes are at the same level along *c*, separated by about 11.4 nm (Figure 11b).[8,13] This means that, in the compact structure of A-amylose, 4 out of 6 neighboring chains are translated by *c*/2 while the other two lie at the same level (supplementary Figure S7). The packing is thus maximized along the *a*-axis. Along the *b*-axis, the repulsion due to the steric hindrance between two double helices at the same level prevents them from getting closer to each other. The distance of equilibrium increases with increasing amplitude of thermal vibrations, resulting in a significant thermal expansion along the *b*-direction. This probably explains why the lateral thermal expansion of A-amylose crystals is highly anisotropic, with a higher amplitude along the *b*-axis (Figure 11d).

The B→A transition can be described as a compaction of the packing of double helices at the cost of a slightly higher inter-helix interaction since, in B-amylose, each double helix has three neighboring chains with complementary surface, whereas in A-amylose, two out of the six neighboring double helices lie at the same height and cannot get closer to each other. In B-amylose, water molecules are expected to fill the volume in the center of six hexagonally-packed double helices (Figure 11a). Upon heating, the entropic penalty due to the restrained freedom of water molecules in the crystal increases, favoring the demixing of water from the crystal lattice. However, this can only happen when the double helices gain enough mobility. In our experiments with amylose spherocrystals, the fact that a higher pressure or an excess of water tended to decrease the B→A transition temperature suggests that the driving force was not the vaporization of water. A higher pressure would rather limit water vaporization. Instead, the excess water plasticized the system and promoted the transition. This case resembles that of chitosan, another polysaccharide

whose hydrated allomorph changes into an anhydrous form in the solid state by heating at high temperature in excess water.[57]

Possible transition pathways of amylose in the solid state, partially based upon that previously described by Pérez et al.,[24] are schematized in Figure 12. On heating, the crystal lattice of allomorph B isotropically expands in the plane perpendicular to the chain axis. When the helices gain enough mobility, the structure collapses to allow for a denser packing of helices schematized by a compression perpendicular to one family of $(010)_B$ planes and then a shear along the same $(010)_B$ planes. Two opposite shears are possible, resulting in two monoclinic unit cells differing in chain polarity. As the initial orientation of the double helices along the *c*-axis must be preserved during the transition in the solid state, only the shear shown on the left hand side in Figure 12 results in the parallel-down unit cell reported for A-amylose by Popov et al.[13] Finally, upon cooling, the crystal contracts, promoting a denser packing of the double helices.

Insert Figure 12

Vermeylen et al. reported that, during the B→A transition in potato starch granules, the 9 nm SAXS peak, corresponding to the repeat distance of the amorphous-crystalline lamellae, disappeared.[29] To account for this phenomenon, the authors proposed that after the disruption of allomorph B and during the recrystallization of allomorph A, the double helices did not only reorganize laterally but also translated along the *c*-axis to minimize the strain applied to the branching points. Another explanation to the disappearance of the SAXS peak may also be found in the different calculated crystal densities of A-amylose (1.6 g/cm^3)[13] and B-amylose (1.4 g/cm^3).[9] As the density of B-type native starch is higher than the theoretical density of B-amylose crystals,[58] the branching points or amorphous regions should have a higher density than the average density of the granule. If the electron density of the branched regions is higher than that of B-type crystallites, the contrast will decrease due to the increase in crystal density associated with the B→A transition.

Moreover, while the axial reorganization proposed by Vermeylen et al. would be promoted by the branching points in amylopectin, no axial translation of the duplexes is required to achieve the B→A transition in the case of crystals made of unrestrained independent short-chain linear

amylose, as shown in the scheme of Figure 12. The B→A transition in amylose crystals would thus be different from the I_α-to-I_β [49,59] and III_I-to-I_β [60] solid-state transitions occurring in cellulose microfibrils, during which an axial translation of the chains occurs.

Conclusion

We have studied the structural changes in native starch granules and highly crystalline amylose spherocrystals during heat treatments in a pressure cell. In particular, we have monitored *in situ* the B→A allomorphic transition in hydrated and wet conditions. As our experimental set-up allowed maintaining a sufficient hydration level in the samples, the B→A transition was successfully achieved and general tendencies were revealed.

The B→A transition was as fast in hydrated starch granules as in amylose spherocrystals, occurring in a matter of minutes. Considering the various botanical origins of our specimens and within a range of pressures of 1.5 to 10 MPa, the transition temperature in native starch varied between 90 and 110°C. This temperature decreased with increasing pressure, whereas, at a given pressure, it increased with increasing amylose content. Within the same pressure range, hydrated B-amylose spherocrystals were converted to A-amylose at a higher temperature (125-135°C) than native starch granules. Again, a higher pressure decreased the transition temperature.

Surprisingly, in wet conditions, at 2.0 MPa, the B-amylose-rich spherocrystals did not melt but were first fully converted to A-amylose before dissolving at high temperature. However, the transition temperature was lower than for hydrated samples, suggesting a plasticizing effect of excess water. To our knowledge, this is the first time that a B→A transition is reported in excess water before dissolution of the crystallites. The reason for such a phenomenon is unclear and may find its origin partly in the specific range of DP of the synthetic amylose that was used (20-40), partly in the high crystallinity of the spherocrystals and partly in an effect of the applied pressure that will have to be investigated in more details.

We also believe that this is the first time that thermal expansion coefficients have been reported

for A- and B-amylose crystals. A strong thermal anisotropy was clearly observed for A-amylose, the expansion being higher along the *b*-axis of the monoclinic unit cell.

During this study, we have tested several sets of environmental parameters but in order to fit within the allocated beamtime at ESRF, we only carried out one or two runs for each set. We should thus consider these experiments as exploratory. Work is in progress to monitor the B→A transition in highly crystalline and pure B-amylose samples using an X-ray diffractometer equipped with an environmental chamber. Analyzing diffraction profiles with a high angular resolution should reveal finer structural details on the structural transition.

Acknowledgement

These experiments were conducted with the financial support of ESRF (proposal SC-1975) and the French CRG (proposal 02-01-670). We thank E. Bertoft (Turku University) and A. Blennow (Copenhagen University) for the gift of PAPS and Dianella samples, respectively, as well as S. Kitamura (Osaka Prefecture University) for providing a sample of synthetic amylose. We are grateful to C. D'Hulst (Lille University) and B. Pontoire (INRA, Nantes) for the determination of the chemical and allomorphic composition of banana starch. The help of N. Follain, M. Cardoso and M. Wada during the experiments at ESRF is greatly acknowledged. We also thank D. Dupeyre (CERMAV) for SEM observations, as well as H. Chanzy (CERMAV) and A. Buléon (INRA, Nantes) for the critical reading of the manuscript and helpful suggestions.

Supporting Information Available

Tables summarizing the composition of the native starch granules samples, the transition temperature for all samples and the thermal expansion coefficients of B- and A-amylose. Equations defining the linear thermal coefficients of the crystals. SEM and polarized optical micrographs of banana and low- and high-amylose Daniella potato starch granules before and after HM treatment. Comparison of the synchrotron X-ray diffraction diagrams recorded from all samples at room temperature before and after HM treatment. Optical micrographs of bubbles trapped in the cavities of

the HM-treated starch granules. Plot of the variation of the unit cell volume of allomorphs B and A with temperature. Molecular structure of A-amylose. This material is available free of charge via the Internet at http://pubs.acs.org.

References

(1) Buléon, A.; Colonna, P.; Planchot, V.; Ball, S. *Int. J. Biol. Macromol.* **1998**, *23*, 85–112.

(2) French, D. *Dempun Kagaku* **1972**, *19*, 8–25.

(3) Robin, J. P.; Mercier, C.; Charbonnière, R.; Guilbot, A. *Cereal Chem.* **1974**, *51*, 389–406.

(4) Jenkins, P. J.; Donald, A. M. *Int. J. Biol. Macromol.* **1995**, *17*, 315–321.

(5) Buléon, A.; Véronèse, G.; Putaux, J.-L. *Aust. J. Chem.* **2007**, *60*, 706–718.

(6) Wu, H.-C. H.; Sarko, A. *Carbohydr. Res.* **1978**, *61*, 7–25.

(7) Wu, H.-C. H.; Sarko, A. *Carbohydr. Res.* **1978**, *61*, 27–40.

(8) Imberty, A.; Chanzy, H.; Pérez, S.; Buléon, A.; Tran, V. *J. Mol. Biol.* **1988**, *201*, 365–378.

(9) Imberty, A.; Pérez, S. *Biopolymers* **1988**, *27*, 1205–1221.

(10) Takahashi, Y.; Kumano, T.; Nishikawa, S. *Macromolecules* **2004**, *37*, 6827–6832.

(11) Imberty, A.; Chanzy, H.; Pérez, S.; Buléon, A.; Tran, V. *Macromolecules* **1987**, *20*, 2634–2636.

(12) Popov, D.; Burghammer, M.; Buléon, A.; Montesanti, N.; Putaux, J.-L.; Riekel, C. *Macromolecules* **2006**, *39*, 3704–3706.

(13) Popov, D.; Buléon, A.; Burghammer, M.; Chanzy, H.; Montesanti, N.; Putaux, J.-L.; Potocki-Véronèse, G.; Riekel, C. *Macromolecules* **2009**, *42*, 1167–1174.

(14) Sair, L. *Cereal Chem.* **1967**, *44*, 8–26.

(15) Stute, R. *Starch/Stärke* **1992**, *44*, 205–14.

(16) Hoover, R.; Vasanthan, T. *Carbohydr. Res*. **1994**, *252*, 33–53.

(17) Jacobs, H.; Delcour, J. A. *J. Agric. Food Chem*. **1998**, *46*, 2895–2905.

(18) Svegmark, K.; Helmersson, K.; Nilsson, G.; Nilsson, P.-O.; Andersson, R.; Svensson, E. *Carbohydr. Polym*. **2002**, *47*, 331–340.

(19) Maruta, I.; Kurahashi, Y.; Takano, R.; Hayashi, K.; Yoshino, Z.; Komaki, T.; Hara, S. *Starch/Stärke* **1994**, *46*, 177–181.

(20) Maache-Rezzoug, Z.; Zarguili, I.; Loisel, C.; Queveau, D.; Buléon, A. *Carbohydr. Polym*. **2008**, *74*, 802–812.

(21) Buléon, A.; Bail, P. L.; Colonna, P.; Bizot, H. In *ISOPOW 6*; Reid, D. S., Ed.; Blackie Academic and Professional, 1998; Chapter Phase and polymorphic transitions of starches at low and intermediate water contents, pp 160–178.

(22) Le Bail, P.; Bizot, H.; Buléon, A. *Carbohydr. Polym*. **1993**, *21*, 99–104.

(23) Katopo, H.; Song, Y.; Jane, J. *Carbohydr. Polym*. **2002**, *47*, 233–244.

(24) Pérez, S.; Imberty, A.; Scaringe, R. P. In *ACS Symposium Series, 430*; French, A. D., Brady, J. W., Eds.; American Chemical Society, Washington DC, 1990; Chapter Computer modeling of carbohydrate molecules, pp 281–299.

(25) Garcia, V.; Colonna, P.; Lourdin, D.; Buléon, A.; Bizot, H.; Ollivon, M. *J. Therm. Anal*. **1996**, *47*, 1213–1228.

(26) Jenkins, P. J.; Donald, A. M. *Carbohydr. Res*. **1998**, *308*, 133–147.

(27) Vermeylen, R.; Derycke, V.; Delcour, J. A.; Goderis, B.; Reynaers, H.; Koch, M. H. J. *Biomacromolecules* **2006**, *7*, 2624–2630.

(28) Vermeylen, R.; Goderis, B.; Delcour, J. A. *Carbohydr. Polym.* **2006**, *64*, 364–375.

(29) Vermeylen, R.; Derycke, V.; Delcour, J. A.; Goderis, B.; Reynaers, H.; Koch, M. H. J. *Biomacromolecules* **2006**, *7*, 1231–1238.

(30) Le Bail, P.; Bizot, H.; Ollivon, M.; Keller, G.; Bourgaux, C.; Buléon, A. *Biopolymers* **1999**, *50*, 99–110.

(31) Bertoft, E. *Starch/Stärke* **2004**, *56*, 167–180.

(32) Blennow, A.; Hansen, M.; Schulz, A.; Jørgensen, K.; Donald, A. M.; Sanderson, J. *J. Struct. Biol.* **2003**, *143*, 229–241.

(33) Wattebled, F.; Dong, Y.; Dumez, S.; Delvallé, D.; Planchot, V.; Berbezy, P.; Vyas, D.; Colonna, P.; Chatterjee, M.; Ball, S.; D'Hulst, C. *Plant Physiol.* **2005**, *138*, 184–195.

(34) Pohu, A.; Planchot, V.; Putaux, J.-L.; Colonna, P.; Buléon, A. *Biomacromolecules* **2004**, *5*, 1792–1798.

(35) Kitamura, S.; Yunokawa, H.; Mitsuie, S.; Kuge, T. *Polym. J.* **1982**, *14*, 93–99.

(36) Testemale, D.; Argoud, R.; Geaymond, O.; Hazemann, J.-L. *Rev. Sci. Instr.* **2005**, *76*, 043905.

(37) Bruyère, R.; Prat, A.; Goujon, C.; Hazemann, J.-L. *J. Phys.: Conf. Ser.* **2008**, *121*, 122003.

(38) von der Linden, W.; Dose, V.; Padayachee, J.; Prozesky, V. *Phys. Rev. E* **1999**, *59*, 6527–6534.

(39) Potocki-Véronèse, G.; Putaux, J.-L.; Dupeyre, D.; Albenne, C.; Remaud-Siméon, M.; Monsan, P.; Buléon, A. *Biomacromolecules* **2005**, *6*, 1000–1011.

(40) Noel, T. R.; Ring, S. G. *Carbohydr. Res.* **1992**, *227*, 203–213.

(41) Morley, M. J.; Miles, C. A. *J. Food. Eng.* **1997**, *33*, 1–14.

(42) Drouzas, A. E.; Saravacos, G. D. *J. Food Sci.* **2006**, *53*, 1795–1799.

(43) Hibi, Y.; Matsumoto, T.; Hagiwara, S. *Cereal Chem*. **1993**, *70*, 671–676.

(44) Błaszczak, W.; Fornal, J.; Kiseleva, V.; Yuryev, V.; Sergeev, A.; Sadowska, J. *Carbohydr. Polym*. **2007**, *68*, 387–396.

(45) Gebhardt, R.; Hanfland, M.; Mezouar, M.; Riekel, C. *Biomacromolecules* **2007**, *8*, 2092–2097.

(46) Buckow, R.; Heinz, V.; Knorr, D. *J. Food. Eng*. **2007**, *81*, 469–475.

(47) Liu, H.; Yu, L.; Dean, K.; Simon, G.; Petinakis, E.; Chen, L. *Carbohydr. Polym*. **2009**, *75*, 395–400.

(48) Kawabata, A.; Takase, N.; Miyoshi, E.; Sawayama, S.; Kimura, T.; Kudo, K. *Starch/Stärke* **1994**, *46*, 463–469.

(49) Debzi, E. M.; Chanzy, H.; Sugiyama, J.; Tekely, P.; Excoffier, G. *Macromolecules* **1991**, *24*, 6816–6822.

(50) Whittam, M. A.; Noel, T. R.; Ring, S. G. *Int. J. Biol. Macromol*. **1990**, *12*, 359–362.

(51) Ring, S. G.; Miles, M. J.; Morris, V. J.; Turner, R.; Colonna, P. *Int. J. Biol. Macromol*. **1987**, *9*, 158–160.

(52) Moates, G. K.; Noel, T. R.; Parker, R.; Ring, S. G. *Carbohydr. Res*. **1997**, *298*, 327–333.

(53) Crochet, P.; Beauxis-Lagrave, T.; Noel, T. R.; Parker, R.; Ring, S. G. *Carbohydr. Res*. **2005**, *340*, 107–113.

(54) Ohashi, Y.; Burnham, C. W. *Am. Mineralogist* **1973**, *58*, 843–849.

(55) Hori, R.; Wada, M. *Cellulose* **2005**, *12*, 479–484.

(56) Wada, M. *J. Polym. Sci., Part B: Polym. Phys*. **2002**, *40*, 1095–1102.

(57) Ogawa, K.; Hirano, S.; Miyanishi, T.; Yui, T.; Watanabe, T. *Macromolecules* **1984**, *17*, 973–975.

(58) Haine, V.; Bizot, H.; Buléon, A. *Carbohydr. Polym.* **1985**, *5*, 91–106.

(59) Wada, M.; Kondo, T.; Okano, T. *Polym. J.* **2003**, *35*, 155–159.

(60) Wada, M.; Heux, L.; Isogai, A.; Nishiyama, Y.; Chanzy, H.; Sugiyama, J. *Macromolecules* **2001**, *34*, 1237–1243.

Figure captions

Figure 1. PAPS (a,b - bars: 20 μm) and Eurylon (c,d - bars: 10 μm) native starch granules; e,f) spherocrystals from DP 20-40 synthetic amylose (bars: 10 μm). a,c,e: SEM images; b,d,f: polarized light micrographs recorded with a λ compensator.

Figure 2. a) Sample holder with a glass capillary containing the hydrated or wet starch powder. Water is placed around the capillary without contact with the powder; b) sapphire cell containing the sample holder; c) picture of the experimental set-up at ESRF showing the pressure cell.

Figure 3. Series of WAXS profiles collected in situ during heat-moisture treatments of native starch granules: a) PAPS at 8.5 MPa; b) PAPS at 1.6 MPa ; c) low-amylose Dianella starch at 8.8 MPa; d) high-amylose Dianella starch at 8.8 MPa; e) Eurylon starch at 11.0 MPa; f) banana starch at 9.2 MPa. For clarity, only selected profiles have been drawn.

Figure 4. Variation of the 100B peak intensity during heat treatments of hydrated native starch granules. Both Dianella starch samples have been treated at 8.8 MPa whereas Eurylon and banana starch have been pressurized at 11.0 and 9.2 MPa, respectively.

Figure 5. PAPS granules after heat-moisture treatments up to 120°C at 1.6 MPa (a,b) and 8.5 MPa (c,d); e,f) Eurylon starch granules after a heat moisture treatment up to 140°C at 11.0 MPa. a,c,e: SEM images; b,d,f: polarized light micrographs recorded with a λ compensator. White arrows in b and d point to cavities around the hilum of some granules. All scale bars : 20 μm.

Figure 6. I and IV) WAXS profiles recorded at room temperature from initial hydrated amylose spherocrystals (peaks indicated by arrows could not be assigned to B-amylose) and after conversion to pure A-amylose, respectively; II) B-type profile calculated by subtracting profile IV from profile I; III, V and VI) profiles calculated from the molecular models proposed by Imberty and Pérez,[24] Imberty et al.,[9] and Popov et al.,[13] respectively.

Figure 7. Series of WAXS profiles recorded during heating of amylose spherocrystals in hydrated and wet conditions: a) 8.5 MPa, hydrated; b) 28.5 MPa, hydrated; c) 2.0 MPa, hydrated; d) 2.0 MPa, wet. For clarity, only selected profiles have been drawn.

Figure 8. Variation of the 100_B peak intensity during heat treatments of hydrated (hyd) and wet amylose spherocrystals at various pressures.

Figure 9. Amylose spherocrystals after heat treatments in hydrated (a,b) and wet (c,d) conditions. Details about each treatment are given in the text. a,c: SEM images (scale bars: 5 μm); b,d: polarized light micrographs recorded with a λ compensator (scale bars: 10 μm).

Figure 10. Variation of the unit cell parameters of allomorphs B (left) and A (right) in amylose spherocrystals with temperature. The data of the four experiments described in the text have been superimposed. Lozenge, circular and square symbols correspond to the experiments carried out on hydrated samples at 2.0, 8.5 and 28.5 MPa, respectively. Solid and empty symbols correspond to heating and cooling treatments, respectively. "+" symbols correspond to the heating of wet spherocrystals at 2.0 MPa.

Figure 11. a,b) Projection of B- and A-amylose lattices, respectively, along the *c*-axis. The cross-section of the doubles helices at position 0 and 1/2 along *c* are drawn as white and grey disks, respectively. c,d) Projections of the thermal expansion ellipsoids deduced from the various experiments and superimposed over the unit cells of B- and A-amylose, respectively. In c: T<140°C; in d: the ellipses correspond to experiments carried out at 2.0 and 8.5 MPa (1), T<120°C, 28.5 MPa (2), 120°C<T<160°C, 28.5 MPa (3) (see supplementary Table S3).

Figure 12. Schematic description of the B→A transition. Only displacements in the *(a,b)* plane are involved. The white and gray disks represent double helices in positions 0 and 1/2, respectively,

along the c-axis, whereas the dotted lined correspond to the projected unit cells. For clarity, the slight increase in helix diameter has not been drawn. Details about each step of the transition are given in the text.

FIGURES

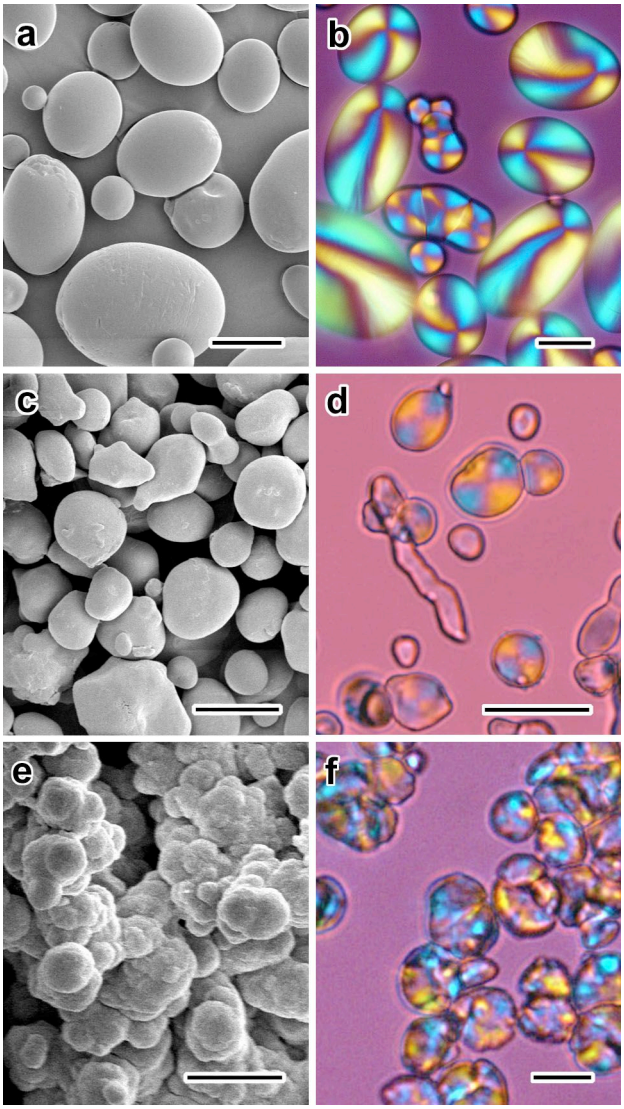

Figure 1. PAPS (a,b - bars: 20 µm) and Eurylon (c,d - bars: 10 µm) native starch granules; e,f) spherocrystals from DP 20-40 synthetic amylose (bars: 10 µm). a,c,e: SEM images; b,d,f: polarized light micrographs recorded with a λ compensator.

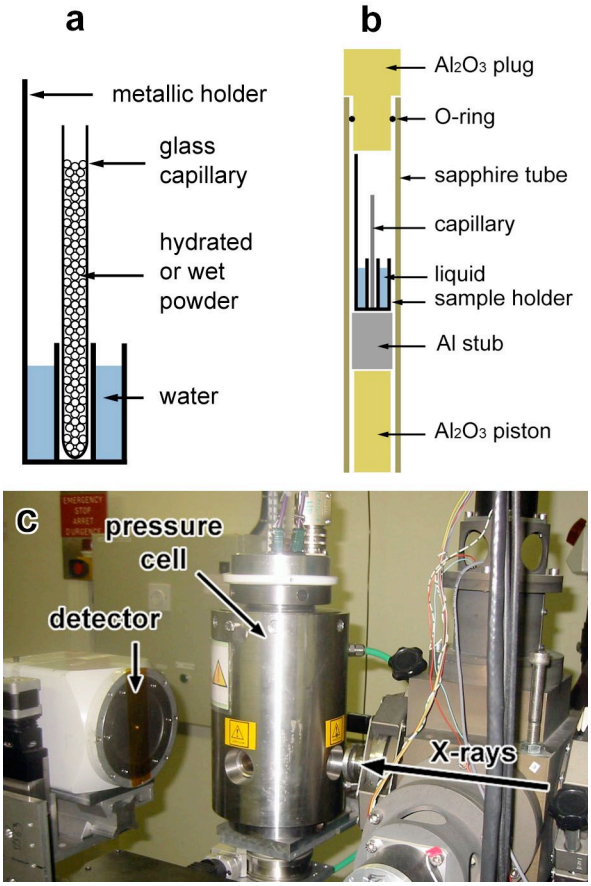

Figure 2. a) Sample holder with a glass capillary containing the hydrated or wet starch powder. Water is placed around the capillary without contact with the powder; b) sapphire cell containing the sample holder; c) picture of the experimental set-up at ESRF showing the pressure cell.[36]

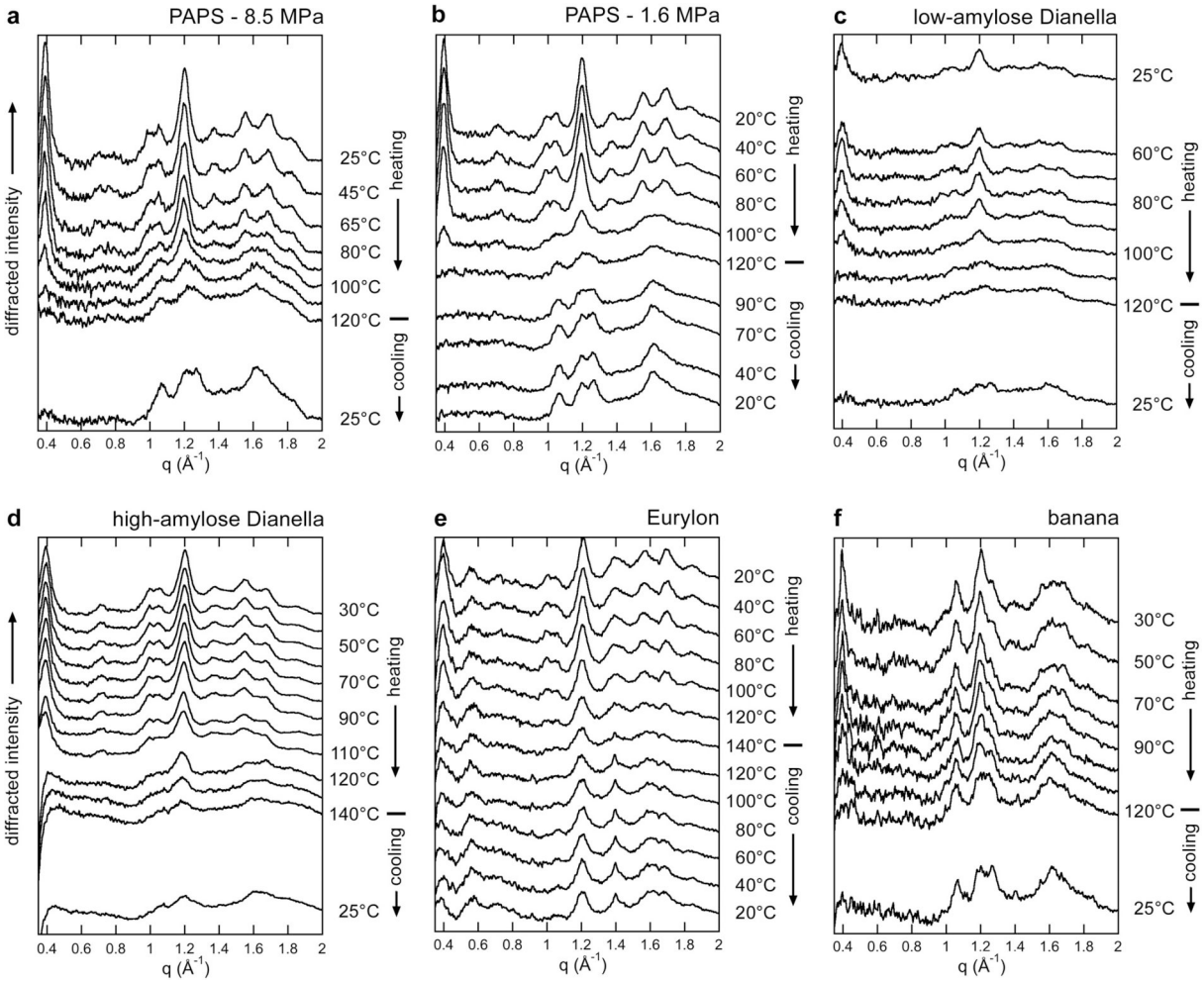

(to be displayed over two columns)

Figure 3. Series of WAXS profiles collected *in situ* during heat-moisture treatments of native starch granules: a) PAPS at 8.5 MPa; b) PAPS at 1.6 MPa ; c) low-amylose Dianella starch at 8.8 MPa; d) high-amylose Dianella starch at 8.8 MPa; e) Eurylon starch at 11.0 MPa; f) banana starch at 9.2 MPa. For clarity, only selected profiles have been drawn.

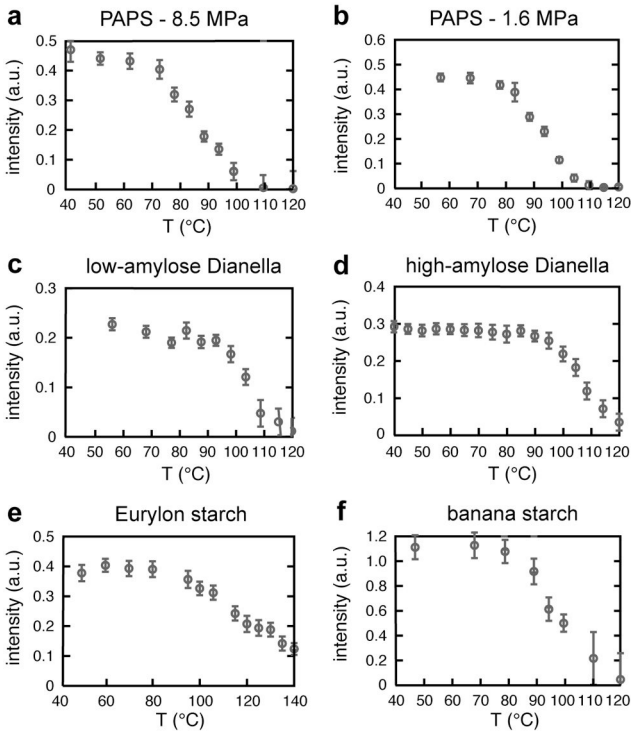

Figure 4. Variation of the 100_B peak intensity during heat treatments of hydrated native starch granules. Both Dianella starch samples have been treated at 8.8 MPa whereas Eurylon and banana starch have been pressurized at 11.0 and 9.2 MPa, respectively.

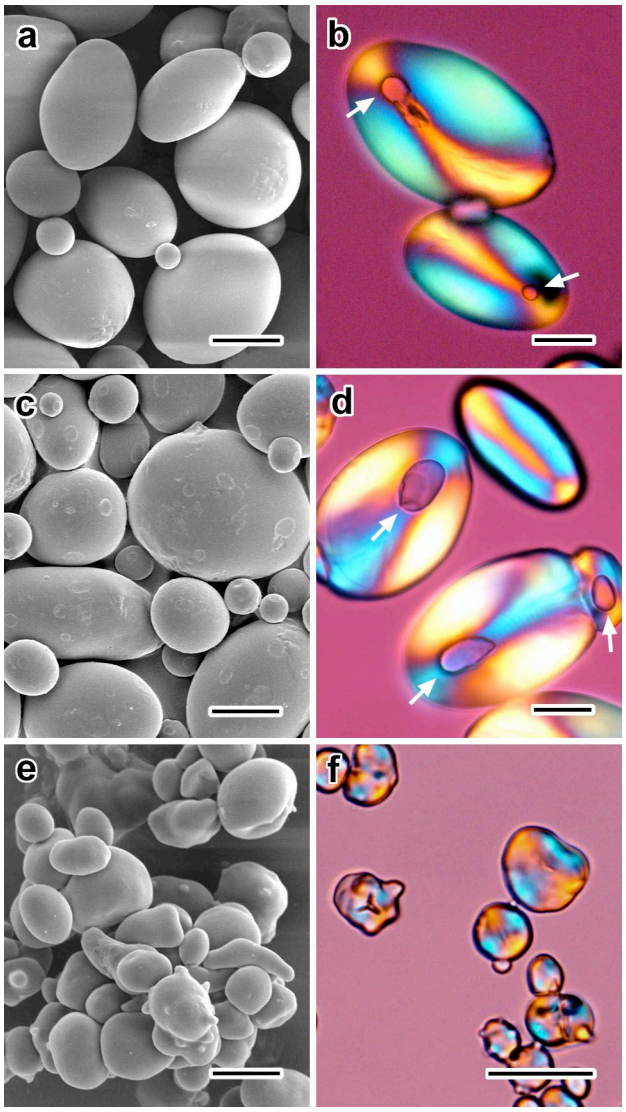

Figure 5. PAPS granules after heat-moisture treatments up to 120°C at 1.6 MPa (a,b) and 8.5 MPa (c,d); e,f) Eurylon starch granules after a heat-moisture treatment up to 140°C at 11.0 MPa. a,c,e: SEM images; b,d,f: polarized light micrographs recorded with a λ compensator. White arrows In b and d point to cavities around the hilum of some granules. All scale bars : 20 µm.

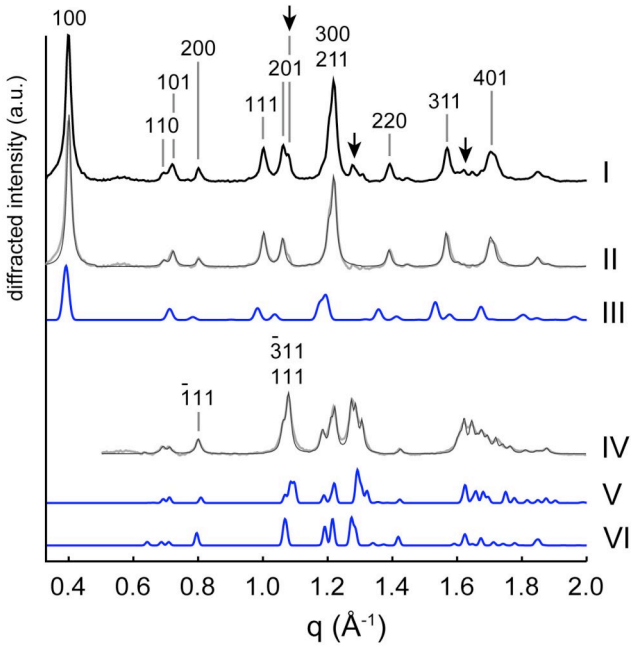

Figure 6. I and IV) WAXS profiles recorded at room temperature from initial hydrated amylose spherocrystals (peaks indicated by arrows could not be assigned B-amylose) and after conversion to pure A-amylose, respectively; II) B-type profile calculated by subtracting profile IV from profile I; III, V and VI) profiles calculated from the molecular models proposed by Imberty and Pérez,[9] Imberty et al.,[8] and Popov et al.,[13] respectively.

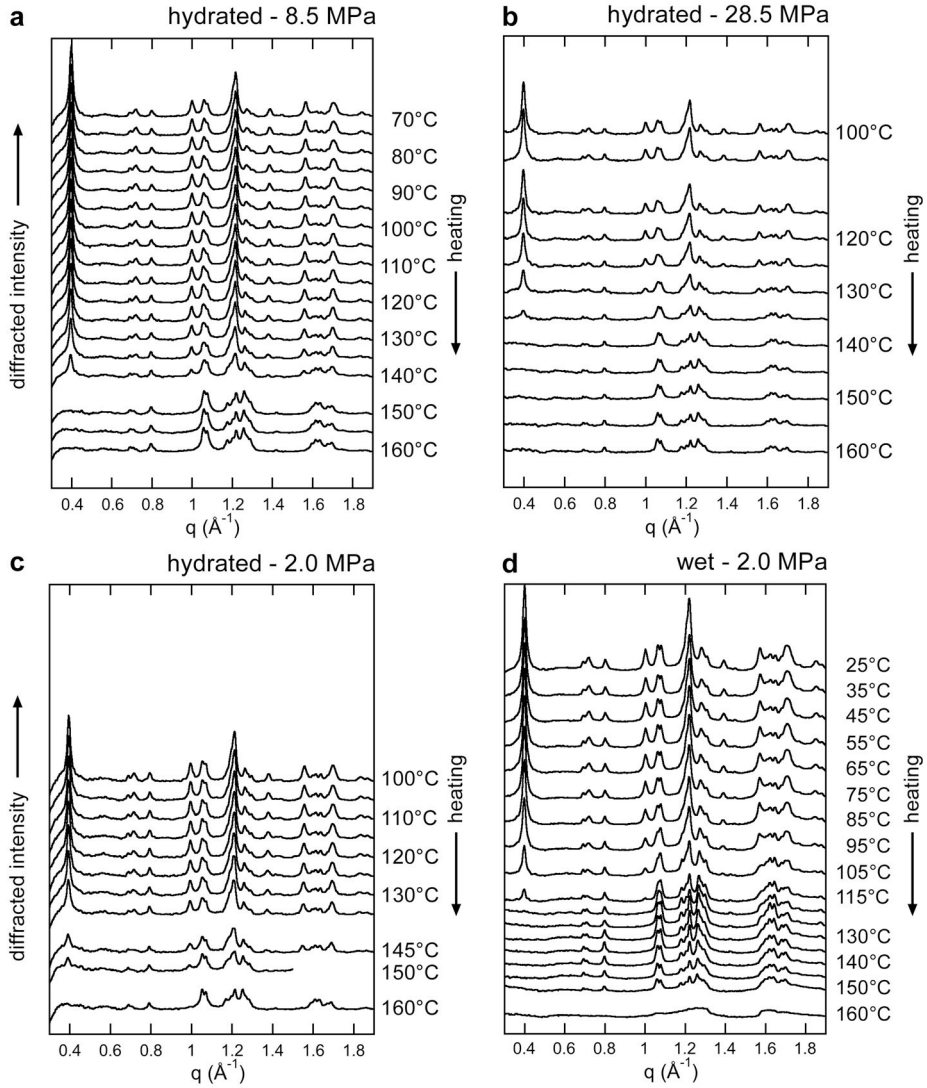

(to be displayed over two columns)

Figure 7. Series of WAXS profiles recorded during heating of amylose spherocrystals in hydrated and wet conditions: a) 8.5 MPa, hydrated; b) 28.5 MPa, hydrated; c) 2.0 MPa, hydrated; d) 2.0 MPa, wet. For clarity, only selected profiles have been drawn.

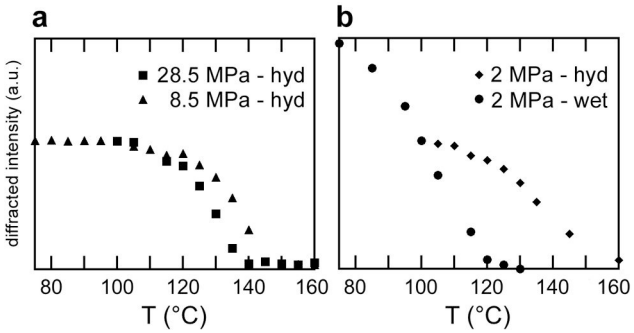

Figure 8. Variation of the 100_B peak intensity during heat treatments of hydrated (hyd) and wet amylose spherocrystals at various pressures.

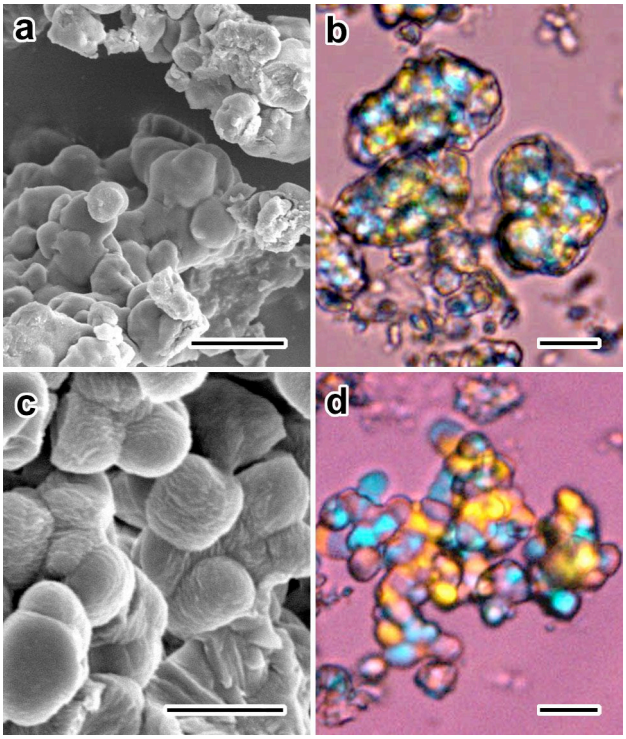

Figure 9. Amylose spherocrystals after heat treatments in hydrated (a,b) and wet (c,d) conditions. Details about each treatment are given in the text. a,c: SEM images (scale bars: 5 µm); b,d: polarized light micrographs recorded with a λ compensator (scale bars: 10 µm).

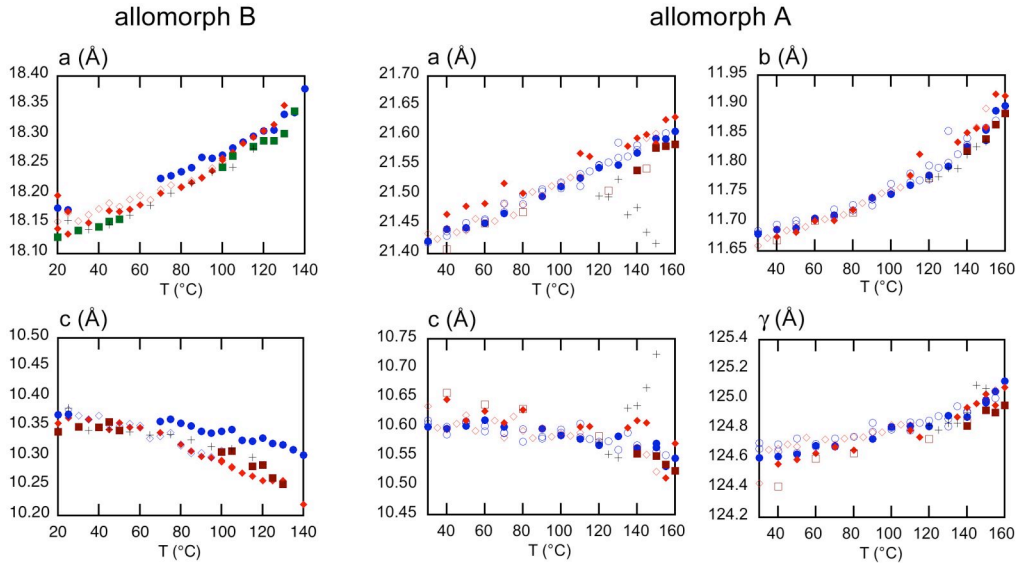

(to be displayed over two columns)

Figure 10. Variation of the unit cell parameters of allomorphs B (left) and A (right) in amylose spherocrystals with temperature. The data of the four experiments described in the text have been superimposed. Lozenge, circular and square symbols correspond to the experiments carried out on hydrated samples at 2.0, 8.5 and 28.5 MPa, respectively. Solid and empty symbols correspond to heating and cooling treatments, respectively. "+" symbols correspond to the heating of wet spherocrystals at 2.0 MPa.

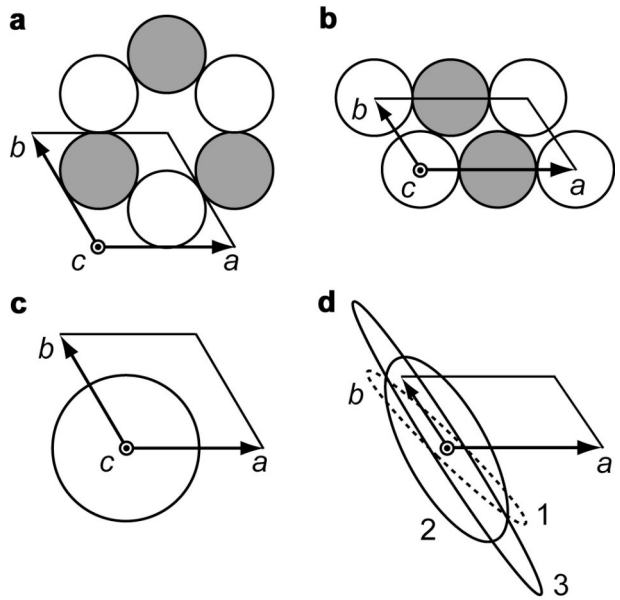

Figure 11. a,b) Projection of B- and A-amylose lattices, respectively, along the *c*-axis. The cross-section of the doubles helices at position 0 and 1/2 along *c* are drawn as white and grey disks, respectively. c,d) Thermal expansion ellipses calculated from the various experiments and superimposed over the unit cells of B- and A-amylose, respectively. In c: T<140°C; in d: the ellipses correspond to experiments carried out at 2.0 and 8.5 MPa (1), T<120°C, 28.5 MPa (2), 120°C<T<160°C, 28.5 MPa (3) (see supplementary Table S3).

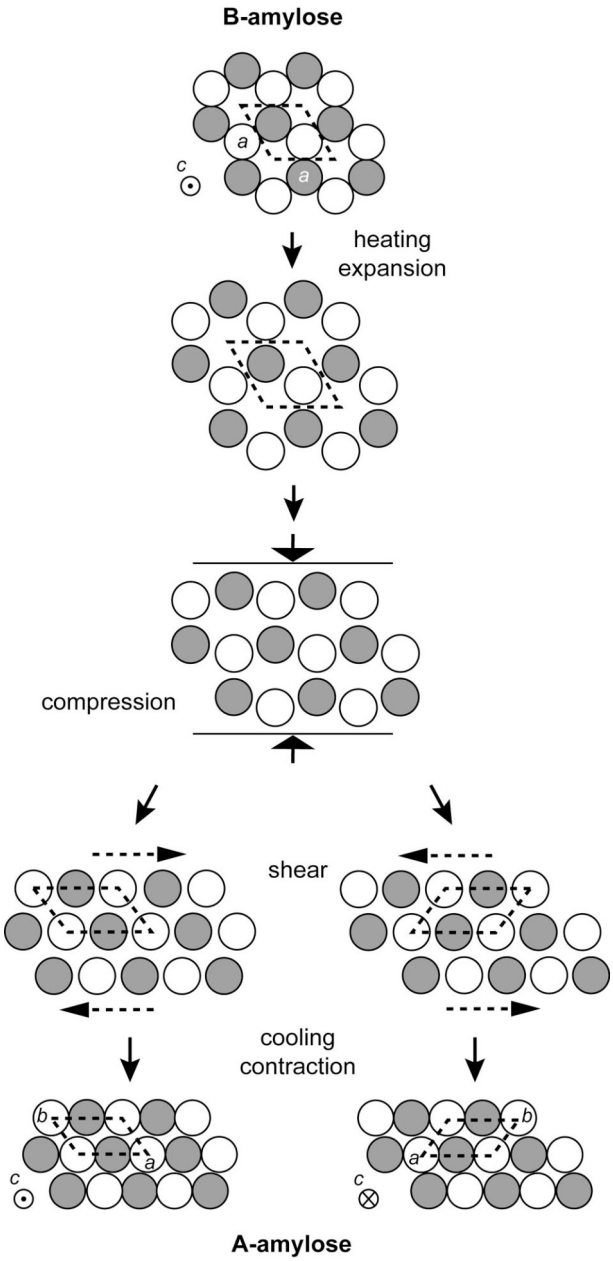

Figure 12. Schematic description of the B→A transition. Only displacements in the (*a,b*) plane are involved. The white and gray disks represent double helices in positions 0 and 1/2, respectively, along the *c*-axis, whereas the dotted lined correspond to the projected unit cells. For clarity, the slight increase in helix diameter has not been drawn. Details about each step of the transition are given in the text.

FOR TABLE OF CONTENTS USE ONLY

B→A allomorphic transition in native starch and amylose spherocrystals monitored by *in situ* synchrotron X-ray diffraction
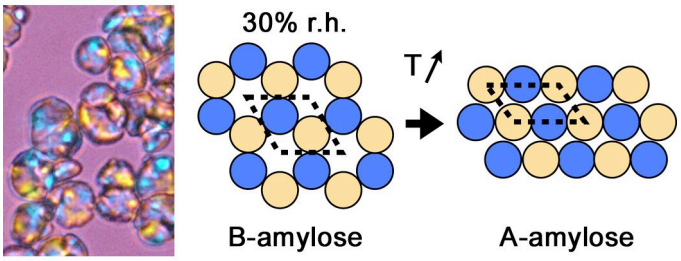
Y. Nishiyama, J.-L. Putaux, N. Montesanti, J.-L. Hazemann, C. Rochas